Article

Structure and Bonding in β-HMX-Characterization of a Trans-Annular N···N Interaction

Elizabeth A. Zhurova, Vladimir V. Zhurov, and A. Alan Pinkerton

J. Am. Chem. Soc., **2007**, 129 (45), 13887-13893• DOI: 10.1021/ja073801b • Publication Date (Web): 16 October 2007

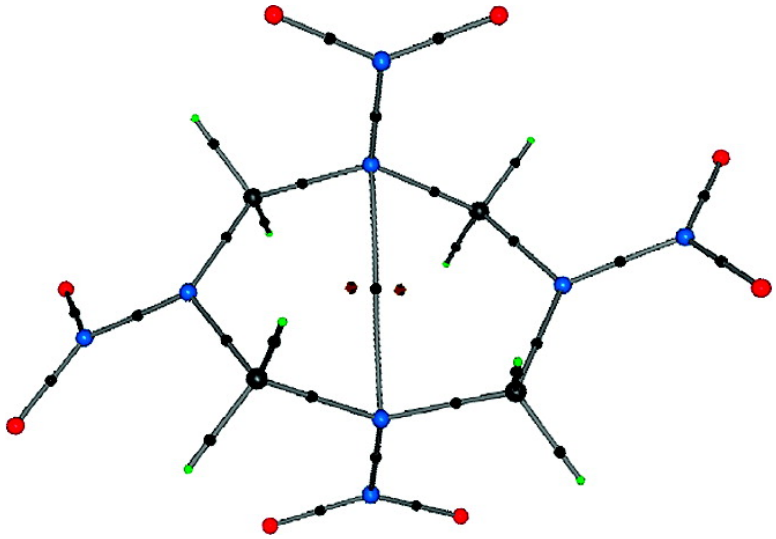

More About This Article

Additional resources and features associated with this article are available within the HTML version:

- Supporting Information
- Links to the 1 articles that cite this article, as of the time of this article download
- Access to high resolution figures
- Links to articles and content related to this article
- Copyright permission to reproduce figures and/or text from this article

View the Full Text HTML

J|A|C|S
ARTICLES
Published on Web 10/16/2007

Structure and Bonding in β-HMX-Characterization of a Trans-Annular N···N Interaction

Elizabeth A. Zhurova, Vladimir V. Zhurov, and A. Alan Pinkerton*

Contribution from the Department of Chemistry, University of Toledo, Toledo, Ohio 43606

Received May 25, 2007; E-mail: apinker@uoft02.utoledo.edu

Abstract: Chemical bonding in the β-phase of the 1,3,5,7-tetranitro-1,3,5,7-tetraazacyclooctane (HMX) crystal based on the experimental electron density obtained from X-ray diffraction data at 20 K, and solid state theoretical calculations, has been analyzed in terms of the quantum theory of atoms in molecules. Features of the intra- and intermolecular bond critical points and the oxygen atom lone-pair locations are discussed. An unusual N···N bonding interaction across the 8-membered ring has been discovered and characterized. Hydrogen bonding, O···O and O···C intermolecular interactions are reported. Atomic charges and features of the electrostatic potential are discussed.

Introduction

There is a continuing interest in the development of new energetic materials and understanding of the behavior of existing explosives based on their microscopic properties.[1] 1,3,5,7-tetranitro-1,3,5,7-tetraazacyclooctane (cyclotetramethylene tetranitramine, HMX)

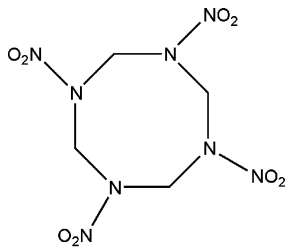

HMX

is one of the most widely used ingredients in various propellants[2] and in several high-performance plastic-bonded explosives.[3] It is a moderately shock sensitive material (h_{50} = 26, 29, 32 cm[4−6]), which makes it a suitable object for an X-ray diffraction study. Crystalline HMX exists in four different polymorphs, known as the α, β, γ, and δ forms. The stable form at room temperature and down to very low temperatures is β-HMX. Crystals have $P2_1/c$ ($P2_1/n$) symmetry with 2 molecules in the unit cell.[7−9] The α-HMX crystal ($Fdd2$, Z = 8) exists in the temperature range 376−435 K.[8] The δ-polymorph ($P6_1$, Z = 6) is stable above 433 K up to the melting point (553 K).[10] The γ-polymorph (Pn, Z = 2) is a hydrate and is metastable at all temperatures at atmospheric pressure.[11] The HMX molecular conformation is different in all four phases: β-HMX has a center of symmetry and the α-form possesses a crystallographic 2-fold axis, whereas the γ and δ forms obey 2-fold symmetry only approximately. The ring conformation of the HMX molecule in the β-form can be described as a chair conformation[12] and will be referred to as the "β-HMX molecule" throughout this paper. We present the analysis of the chemical bonding in the β-HMX crystal based on the quantum theory of atoms in molecules (QTAIM).[13] Features of the intra- and intermolecular bond critical points and the oxygen atom lone-pair locations are reported. The deformation electron density and electrostatic potential maps are also discussed.

Experimental

Data Collection and Reduction. A regularly shaped crystal (Table 1), crystallized from hot acetone, was mounted with oil inside a nylon loop (size ~0.3 mm) and cooled to 20 K with an open flow helium cryostat.[14−16] This type of crystal mount allowed us to minimize strain in the crystal that occurred when using a hard epoxy-resin mount, and relatively fast cooling (within a half hour), without a risk of loosing the crystal under the helium flow. The X-ray diffraction measurements were performed with a Rigaku R-Axis Rapid diffractometer with a high-

(1) Politzer, P., Murray, J. S., Eds. *Energetic Materials*; Theoretical and Computational Chemistry Series, Vol. 12; Elsevier: New York, 2003.
(2) Sorescu, D. C.; Rice, B. M.; Thompson, D. L. *J. Phys. Chem. B* **1998**, *102*, 6692−6695.
(3) Gibbs, T. R., Popolato, A., Eds. *LASL Explosive Property Data*; University of California Press: Berkeley, 1980.
(4) The shorter the impact drop height, h_{50}, the greater is the sensitivity.
(5) Storm, C. B.; Stine, J. R.; Kramer, J. F. *Chemistry and Physics of Energetic Materials*; Bulusu, S. N., Ed.; Kluwer Academic Publishers: Norwell, MA, 1990; pp 605−639.
(6) Simpson, R. L.; Urtiew, P. A.; Omellas, D. L.; Moody, G. L.; Scribner, K. J.; Hoffman, D. M. *Propellants, Explos., Pyrotech.* **1997**, *22*, 249−255.
(7) Eiland, P. F.; Pepinsky, R. *Z. Kristallogr.* **1955**, *106*, 273−298.
(8) Cady, H. H.; Larson, A. C.; Cromer, D. T.; *Acta Cryst.* **1963**, *16*, 617−623.
(9) Choi, C. S.; Boutin, H. P. *Acta Cryst.* **1970**, *B26*, 1235−1240.
(10) Cobbledick, R. E.; Small, R. W. H. *Acta Cryst.* **1974**, *B30*, 1918−1922.
(11) Main, P.; Cobbledick, R. E.; Small, R. W. H. *Acta Cryst.* **1985**, *C41*, 1351−1354.
(12) Brill, T. B.; Reese, C. O. *J. Phys. Chem.* **1980**, *84*, 1376−1380.
(13) Bader, R. F. W. *Atoms in Molecules: A Quantum Theory. The International Series of Monographs of Chemistry*; Halpen, J., Green, M. L. H., Eds.; Clarendon Press: Oxford, 1990; p. 1−438.
(14) Hardie, M. J.; Kirschbaum, K.; Martin, A.; Pinkerton, A. A. *J. Appl. Cryst.* **1998**, *31*, 815−817.
(15) Kirschbaum, K.; Martin, A.; Parrish, D.; Pinkerton, A. A. *J. Phys. Condens. Matter* **1999**, *11*, 4483−4490.
(16) Ribaud, L.; Wu, G.; Zhang, Y.; Coppens, P. *J. Appl. Cryst.* **2001**, *34*, 76−79.

Table 1. Experimental Details

empirical formula	$C_4H_8O_8N_8$
temperature (K)	20(2)
crystal size (mm)	0.26 × 0.26 × 0.12
crystal shape	prism
wavelength (Å)	0.71073
crystal system	monoclinic
space group	$P2_1/n$
unit cell dimensions (Å)	$a = 6.5209(2)$, $b = 10.7610(2)$, $c = 7.3062(2)$, $\beta = 102.058(2)$
V (Å^3), Z	501.37, 2
μ (mm^{-1})	0.19
$(\sin\theta/\lambda)_{max}$ (Å^{-1})	1.327
reflections integrated ($I > 3\sigma$)	32880
R_{int} /average data multiplicity	0.0164/8.1
completeness ($I > 3\sigma$):	
sin $\theta/\lambda < 0.5$ Å^{-1}, %	92.6
all data, %	41.2
independent reflections	4041
reflections used ($I > 3$s, measured more than 2 times)	3132
refinement based on	F^2
total number of parameters	389
final $R(F^2)$	0.0120
$R_w(F^2)$	0.0181
$R(F)$	0.0111
goodness of fit	1.09
$\Delta\rho_{min/max}$, eÅ^{-3}	−0.12/0.12

power Mo rotating anode generator (18 kW), graphite monochromator, and a curved image plate detector. To obtain sufficient redundancy of data, four complete runs covering 0−180° in ω were collected at different χ and φ settings, two at $\chi = 0$ ($\varphi = 0$, 180°) and two at $\chi = 20°$ ($\varphi = 0$, 180°). To avoid significant overlap of reflections in any one image, a 4° ω-scan range was chosen. Oscillation ranges for adjacent images overlapped by 2° to provide precise scaling between them. Thus, each run consisted of a total of 89 images. An exposure time of 70 s per image was chosen to maximize scattering power and avoid saturation of the strongest reflections. The measurement was completed in ~19 h.

The collected data were integrated with the program VIIPP[17,18] using the predicted reflection positions from the program HKL2000.[19] Reflections below $3\sigma(I)$ were rejected during the integration, as well as partial and overlapped reflections. Data have been corrected for the Lorentz-polarization effect. Effects of absorption ($\mu = 0.19$ mm^{-1}) and thermal diffuse scattering at 20 K were considered to be negligible. Data were scaled and then averaged in the 2/m point group with the program SORTAV.[20] Most of the scaling factors for different images were very close to unity (usually within 1%, however, in several cases differences of up to 3.3% were observed). Extreme outliers (11 reflections) were rejected during averaging, and reflections measured no more than twice were also discarded from the final data set. Other experimental details are listed in Table 1.

Refinements. The crystal structure of β-HMX was reported previously.[7−9] From our experimental data, the crystal structure was resolved by direct methods and a preliminary least-squares refinement was carried out with the SHELXTL program suite.[21] The positions of hydrogen atoms at this stage were determined from the difference Fourier peaks. Anisotropic thermal motion was considered for all non-hydrogen atoms, and the latter were refined isotropically. A multipole model refinement[22] using the XD program package[23] was performed for both experimental and solid state theoretical (see below) data. All "heavy" atoms have been refined up to the hexadecapole level, whereas the hydrogen atoms were refined up to quadrupoles. Chemical constraints for similar atoms were applied at the initial stages of refinements. Then, these constraints were gradually released, and the final model was refined unconstrained. The molecular electroneutrality requirement has been applied. A total of 5 expansion−contraction parameters, κ and κ', were utilized to allow the necessary flexibility while attempting to maintain a minimum number of parameters. For the theoretical data, all κ and κ' values were freely refined including those for the hydrogen atoms. For the experimental data, κ and κ' values for all hydrogen atoms were fixed to 1.2. The C−H bond lengths were fixed to the tabulated values[24] (1.092 Å). Highly correlated parameters were initially refined in separate groups, the refinement procedure was stable, and full convergence of all parameters has been reached.

Evaluation of Data Quality. A number of statistical measures of data quality obtained from the program *SORTAV* [20] have been deposited. The values for R_{int} and the average $I/\sigma(I)$ in the various resolution shells suggest excellent data quality. The rigid-bond test[25] showed that the differences of mean-square displacement amplitudes along the interatomic vectors were less than 6×10^{-4} Å^2. Averaged ratios (in 0.05 Å^{-1} bins) of observed and calculated structure factors were very close to unity (within 1%) indicating a correct scale factor for all data,[26] as well as good model fitting for the whole sin θ/λ range. The residual electron density (the difference between observed and calculated multipole electron densities: $\delta\rho_{resid} = \rho_{exper} - \rho_{mult}$) showed no peaks above or below 0.12/−0.12 eÅ^{-3} (calculated with all data); maps have been deposited. The total electron density was non-negative everywhere.

A drawing of the β-HMX molecule, showing 50% thermal probability ellipsoids, and a view of the crystal packing are presented in Figures 1 and 2. Layers of molecules perpendicular to the **a**+**c**

(17) Zhurov, V. V.; Zhurova, E. A.; Chen, Y. -S.; Pinkerton, A. A. *J. Appl. Cryst.* **2005**, *38*, 827−829.
(18) Zhurova, E. A.; Zhurov, V. V.; Tanaka, K. *Acta Cryst.* **1999**, *B55*, 917−922.
(19) Otwinowski, Z.; Minor, W. *Methods Enzymol.* **1997**, *276A*, 307−326.
(20) Blessing, R. H. *Cryst. Rev.* **1987**, *1*, 3−58.
(21) Sheldrick, G. M. *SHELXTL Vers.6.14. An Integrated System for Solving, Refining and Displaying Crystal Structures from Diffraction Data*; Univ. of Göttingen: Germany, 2000.
(22) Hansen, N.; Coppens, P. *Acta Cryst.* **1978**, *A34*, 909−921.
(23) Koritsanszky, T.; Richter, T.; Macci, P.; Gatti, C.; Howard, S.; Mallinson, P. R.; Farrugia, L.; Su, Z. W.; Hansen, N. K. *XD − A Computer Program Package for Multipole Refinement and Analysis of Electron Densities from Diffraction Data*; Tech. Rep.; Freie Universität Berlin: Berlin, Germany, 2003.
(24) Allen, F. H.; Kennard, O.; Watson, D. G.; Brammer, L.; Orpen, A. G.; Taylor, R. *J. Chem. Soc. Perkin Trans. 2*, **1987**, S1−S19.
(25) Hirshfeld, F. L. *Acta Cryst.* **1976**, *A32*, 239−244.
(26) In the case of experimental data.

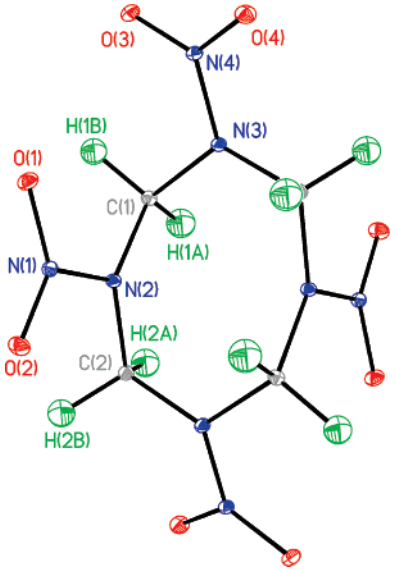

Figure 1. *β*-HMX molecule showing 50% thermal probability ellipsoids at 20 K.

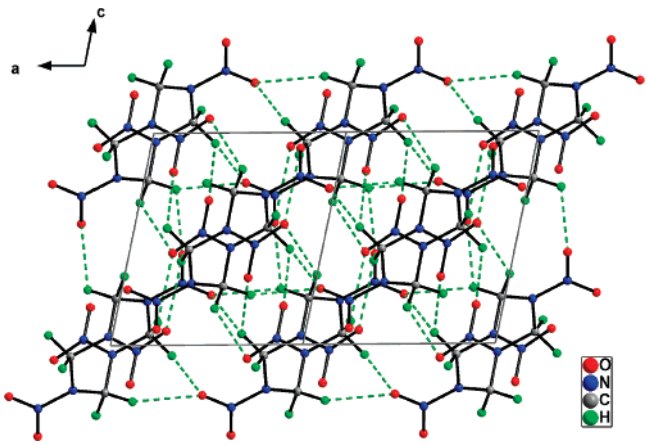

Figure 2. *β*-HMX packing diagram, hydrogen bonds are shown as green dashed lines.

crystallographic direction are clearly observed. For the electron density analysis the program packages XDPROP [23]and WinXPRO[27,28] have been used.

Theoretical Calculations. To verify some of the experimental results, a density functional theory (DFT) B3LYP periodic theoretical calculation was performed with the program CRYSTAL98.[29] The 6-311G(d,p) basis set and a molecular geometry fixed at that observed experimentally were used. The theoretical structure factors have been calculated for all possible *hkl* indices up to sin $\theta/\lambda = 1.0$ Å^{-1}, and used for refinements in the same manner as the experimental data. A final $R(F) = 0.0050$ was reached, and the residual electron density showed no peaks above or below 0.08/−0.11 eÅ^{-3}.

Results and Discussion

A preliminary electron density analysis for *β*-HMX at 90 K has been reported previously.[30] Our current results show, in general, the same tendencies, although demonstrating much better quality. No closed-shell interactions in *β*-HMX have been reported before. The experimental static (model) deformation electron density maps ($\delta\rho = \rho_{\text{multipole}} - \rho_{\text{spherical}}$) and the Laplacian ($\nabla^2\rho$) maps are shown in Figure 3 in the planes of two different NO_2 groups; other maps have been deposited. Each expected covalent bond manifests itself as a significant deformation electron density and negative Laplacian peak. For all four oxygen atoms, electron concentrations associated with lone pairs are well-shaped and located close to perpendicular to the N−O bond vectors. A (3,+3) critical point (CP) search in the Laplacian around the oxygen atoms has been performed; the $\nabla^2\rho$ values vary between −130.0 and −137.6 eÅ^{-5}, and the CP−O−CP angles vary between 160.5 and 163.2°. A very similar picture has been observed for nitro groups in a number of explosive[31−35] and non-explosive materials.[36−38]

Table 2 lists all the intramolecular (3,−1) bond critical points (CP's); for the NO_2 groups, their positions along with the associated bond paths are shown in Figure 3. Generally, good agreement between theory and experiment is observed for the electron density values. For the Laplacian values, the agreement is less satisfying, mostly due to the difference in the λ_3 values related to the deficiency of the multipole model description of the electron density.[39,40] For the covalent bonds, topological bond orders[35,41,42] have been calculated from the electron density values (ρ) and the principle electron-density curvatures (λ_1, λ_2, λ_3) at the bond critical points (Table 2) as $n_{\text{topo}} = a + b\lambda_3 + c(\lambda_1 + \lambda_2) + d\rho_{\text{CP}}$, all values in atomic units. The following coefficients were used: for the N−O bond $a = -0.628$, $b = 0.505$, $c = 0.448$, $d = 5.275$; for the N−N bond $a = -0.755$, $b = 0.525$, $c = 2.041$, $d = 13.432$; for the N−C bond $a = -0.851$, $b = 0.221$, $c = 0.715$, $d = 8.561$; for the C−H bonds $a = -0.153$, $b = 0.481$, $c = 0.983$, $d = 8.087$. Table 2 shows that, according to the bond-order values, the N−C and C−H bonds are single, as expected, with average bond order values of 0.76 and 0.93, respectively. The N−O bond order is 1.89 on average, and the N−N bond order is 1.36, both values reflecting the conjugation of the electron density in the $-N-NO_2$ fragment. The N−N bonds are also significantly polarized and highly elliptical. No chemical reason for the ellipticity of the N(3)−C(2)$^{(1-x,\ -y,\ 1-z)}$ was found; the corresponding deformation density map has been deposited.

It is of interest to compare the $N-NO_2$ bond in the *β*-HMX molecule with $O-NO_2$ and $C-NO_2$ reported previously for other energetic materials.[31,34,35] The N−N bonds have much higher electron density at the critical points (on average, 2.42

(27) Stash, A. I.; Tsirelson, V. G. *J. Appl. Cryst.* **2002**, *35*, 371−373.
(28) Stash, A. I.; Tsirelson, V. G. *Crystallogr. Rep.* **2005**, *50*, 202−209.
(29) Saunders, V. R.; Dovesi, R.; Roetti, C.; Causà, M.; Harrison, N. M.; Orlando, R.; Sicovich-Wilson, C. M. *CRYSTAL98 User's Manual*; University of Torino: Torino, 1998.
(30) Chen, Y.-S. Ph.D. Thesis 2004, University of Toledo, Toledo, OH, U.S.A.
(31) Zhurova, E. A.; Pinkerton, A. A. *Acta Cryst.* **2001**, *B57*, 359−365.
(32) Zhurova, E. A.; Martin, A.; Pinkerton, A. A. *J. Am. Chem. Soc.* **2002**, *124*, 8741−8750.
(33) Ritchie, J. P.; Zhurova, E. A.; Martin, A.; Pinkerton, A. A. *J. Phys. Chem. B* **2003**, *107*, 14576−14589.
(34) Chen, Y.-S.; Stash, A. I.; Pinkerton, A. A. *Acta Cryst.* **2007**, *B63*, 309−318.
(35) Zhurova, E. A.; Stash, A. I.; Tsirelson, V. G.; Zhurov, V. V.; Bartashevich, E. V.; Potemkin, V. A.; Pinkerton, A. A. *J. Am. Chem. Soc.* **2006**, *128*, 14728−14734.
(36) Kubicki, M.; Borowiak, T.; Ditkiewicz, G.; Souhassou, M.; Jelsch, C.; Lecomte, C. *J. Phys. Chem.* **2002**, *106*, 3706−3714.
(37) Volkov, A.; Abramov, Yu.; Coppens, P.; Gatti, C. *Acta Cryst.* **2000**, *A56*, 332−339.
(38) Messerschmidt, M.; Wagner, A.; Wong, M. W.; Luger, P. *J. Am. Chem. Soc.* **2002**, *124*, 732−733.
(39) Volkov, A.; Abramov, Yu.; Coppens, P.; Gatti, C. *Acta Cryst.* **2000**, *A56*, 332−339.
(40) Tsirelson, V. G.; Stash, A. I.; Potemkin, V. A.; Rykounov, A. A.; Shutalev, A. D.; Zhurova, E. A.; Zhurov, V. V.; Pinkerton, A. A.; Gurskaya, G. V.; Zavodnik, V. E. *Acta Cryst.* **2006**, *B62*, 676−688.
(41) Howard, S. T.; Lamarche, O. *J. Phys. Org. Chem.* **2003**, *16*, 133−141.
(42) Tsirelson, V. G.; Bartashevich, E. V.; Stash, A. I.; Potemkin, V. A. *Acta Cryst.* **2007**, *B63*, 142−150.

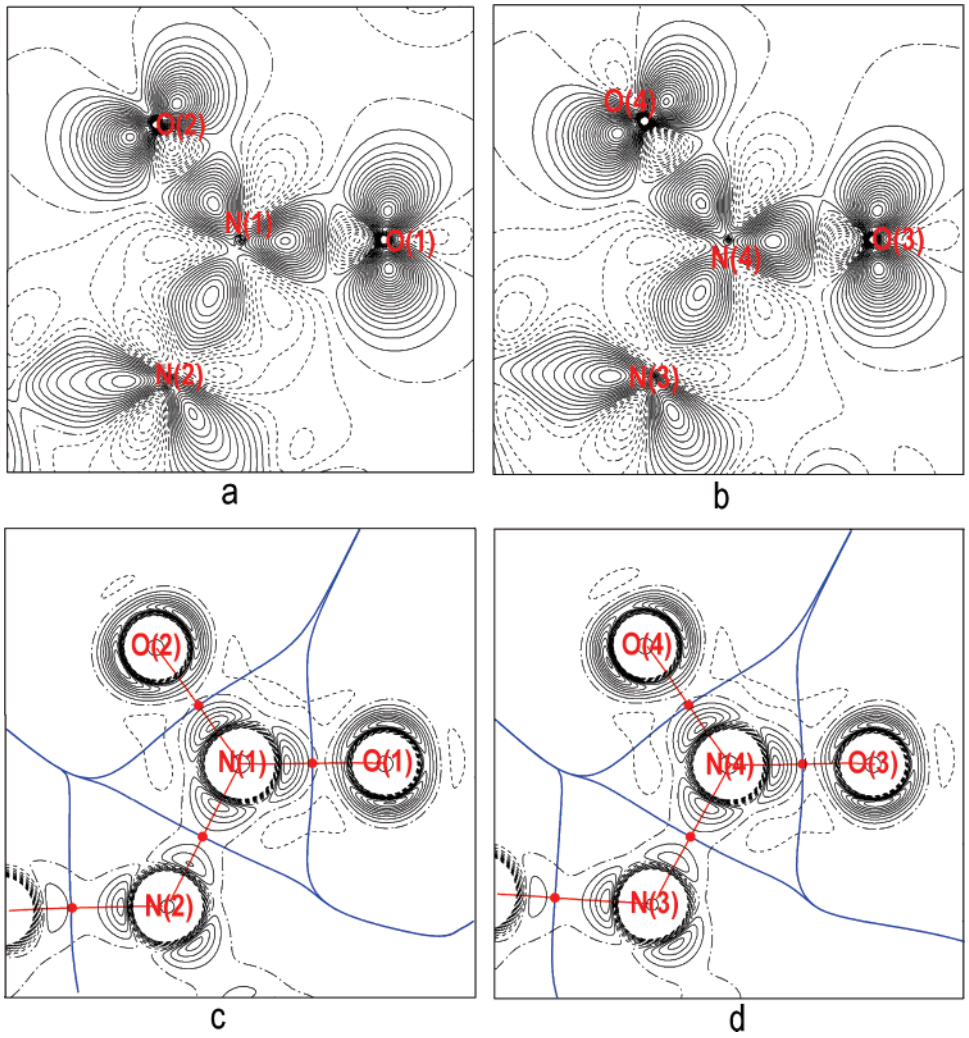

Figure 3. Maps of experimental static deformation electron density (a and b) and Laplacian (c and d) overlapped with projections of zero-flux surfaces (blue) and bond paths (red) in the planes of the NO_2 groups. Contour intervals are 0.05 eÅ^{-3} for the electron density, and 15 eÅ^{-5} for the Laplacian. Black solid contours represent the concentration of the electron density. Bond critical points in the electron density are shown as red circles, (3,−3) points are omitted for clarity.

eÅ^{-3} compared to 2.23 eÅ^{-3} for O−N[35] and 2.05 eÅ^{-3} for C−N[31,34]) and higher bond orders (1.36 for N−N, 1.17 for O−N,[35] and 0.92 for C−N[31,34]) reflecting a decrease in conjugation, $N-NO_2 > O-NO_2 > C-NO_2$.

In addition to regular (covalent) bonds in the β-HMX molecule, a N(2)···N(2)$^{(1-x,\ -y,\ 1-z)}$ interaction (at 2.7444(4) Å) across the 8-membered ring has been found from both experimental and theoretical electron densities. The corresponding critical point properties are listed in Table 2, the energy densities at the CP are shown in Table 3, and the complete molecular graph is presented in Figure 4. The (3,−1) CP, bond path and associated virial path found for this interaction strongly suggest its *bonding* character.[43] The relatively small electron density value at the CP, positive Laplacian and positive electronic energy density (Table 3) are indications of the closed-shell type of this interaction.[44] Although there is no way to directly calculate the stabilization energy provided by this N···N interaction, an approximate estimation of the dissociation energy (Table 3) gives a value of ∼17 kJ/mol (∼4 kcal/mol), which is comparable to a strong hydrogen bond.[32,35] The N(2) atomic charge and total electronic energy (Table 4) are slightly more negative (especially in the theoretical case) than for the chemically "equivalent" N(3) atom, which is not involved in an extra bonding interaction (the N(3)−N(3) interatomic distance is 3.9420(4) Å). At ∼0.266 Å from the bond CP located at the inversion center, associated ring (3,+1) CP's have been found inside each 5-membered ring (Figure 4) as required to satisfy the Poincaré−Hopf−Morse condition.[45] The same interaction has been found from a single molecule calculation with Gaussian98[46] (DFT/B3LYP/6-311G(d,p)) at the experimental geometry (at the CP $\rho = 0.119$ eÅ^{-3}, $\nabla^2\rho = 1.72$ eÅ^{-5}). A molecular calculation with full geometry optimization results in a longer N ··· N distance (2.848 Å) with the CP properties $\rho = 0.098$ eÅ^{-3} and $\nabla^2\rho = 1.39$ eÅ^{-5}. Although rare, similar trans-annular O,S···Sb interactions have been topologically characterized based on theoretical calculations in dibenzostibocines;[47] Sb,Bi···N in azastibatranes and azabismatranes;[48]

(43) Bader, R. F. W. *J. Phys. Chem.* **1998**, *A102*, 7314−7323.
(44) Gatti, C. *Z. Kristallogr.* **2005**, *220*, 399−457.
(45) Martin Pendas, A.; Costales, A.; Luana, V. *Phys. Rev.* **1997**, *B55*, 4275−4284.
(46) Frisch, M. J.; et al. *Gaussian 98*; Gaussian, Inc.: Pittsburgh, PA, 1998.
(47) Alvarado-Rodriguez, J. G.; Andrade-Lopez, N.; Gonzalez-Montiel, S.; Merino, G.; Vela, A. *Eur. J. Inorg. Chem.* **2003**, 3554−3562.
(48) Shutov, P. L.; Karlov, S. S.; Harms, K.; Tyurin, D. A.; Churakov, A. V.; Lorberth, J.; Zaitseva, G. S. *Inorg. Chem.* **2002**, *41*, 6147−6152.

Table 2. Bond Critical Points in the β-HMX Crystal: Intramolecular Bonds[a]

bond	ρ, eÅ^{-3}	$\nabla^2\rho$, eÅ^{-5}	R_{ij}, Å	d_1, Å	d_2, Å	λ_1, eÅ^{-5}	λ_2, eÅ^{-5}	λ_3, eÅ^{-5}	ϵ	n_{topo}
O(1)−N(1)	3.330	−7.34	1.231	0.617	0.614	−30.180	−28.711	51.550	0.051	1.960
	3.247	−11.49	1.231	0.629	0.602	−29.100	−27.237	44.845	0.068	1.803
O(2)−N(1)	3.356	−7.17	1.224	0.617	0.607	−30.325	−28.732	51.891	0.055	1.985
	3.295	−12.02	1.224	0.626	0.598	−29.385	−27.822	45.189	0.056	1.831
O(3)−N(4)	3.348	−6.40	1.226	0.612	0.614	−30.470	−28.249	52.319	0.079	1.994
	3.284	−11.86	1.226	0.626	0.600	−29.277	−27.680	45.100	0.058	1.825
O(4)−N(4)	3.261	−5.82	1.237	0.621	0.615	−29.364	−27.771	51.318	0.057	1.934
	3.202	−10.57	1.237	0.632	0.605	−28.484	−26.822	44.737	0.062	1.784
N(1)−N(2)	2.442	−10.27	1.370	0.705	0.665	−22.930	−17.979	30.635	0.275	1.308
	2.355	−7.84	1.370	0.701	0.669	−21.358	−16.593	30.116	0.287	1.374
N(3) −N(4)	2.481	−10.38	1.363	0.655	0.708	−23.396	−17.803	30.823	0.314	1.365
	2.394	−8.18	1.363	0.665	0.698	−21.776	−16.921	30.521	0.287	1.398
N(2)−C(1)	1.783	−12.34	1.458	0.832	0.627	−13.637	−12.741	14.035	0.070	0.757
	1.737	−9.85	1.458	0.817	0.641	−13.005	−12.030	15.190	0.081	0.749
N(2)−C(2)	1.877	−14.05	1.441	0.817	0.625	−14.437	−13.892	14.278	0.039	0.821
	1.811	−11.71	1.441	0.809	0.632	−13.620	−13.085	14.993	0.041	0.792
N(3)−C(1)	1.814	−12.37	1.457	0.828	0.629	−13.810	−13.087	14.523	0.055	0.785
	1.749	−10.29	1.457	0.817	0.640	−13.127	−12.281	15.117	0.069	0.753
N(3)−C(2)[b]	1.713	−11.06	1.481	0.844	0.637	−13.451	−11.802	14.193	0.140	0.703
	1.669	−8.96	1.481	0.827	0.654	−12.917	−11.202	15.162	0.153	0.690
C(1)−H(1A)	1.935	−22.14	1.092	0.727	0.365	−19.421	−18.657	15.934	0.041	0.931
	1.944	−22.14	1.092	0.730	0.362	−19.783	−19.015	16.660	0.040	0.927
C(1)−H(1B)	1.893	−21.31	1.092	0.748	0.344	−19.427	−18.565	16.678	0.046	0.899
	1.929	−21.19	1.092	0.736	0.356	−19.517	−18.889	17.212	0.033	0.936
C(2)−H(2A)	1.906	−21.08	1.092	0.735	0.357	−19.306	−18.343	16.564	0.053	0.926
	1.931	−21.30	1.092	0.729	0.363	−19.366	−18.833	16.897	0.028	0.940
C(2)−H(2B)	1.898	−21.00	1.092	0.744	0.348	−19.289	−18.521	16.811	0.041	0.915
	1.935	−21.65	1.092	0.734	0.358	−19.639	−18.960	16.953	0.036	0.930
N(2)−N(2)[b]	0.116	1.71	2.744	1.372	1.372	−0.307	−0.055	2.072	−	−
	0.118	1.73	2.744	1.372	1.372	−0.311	−0.099	2.144	−	−

[a] First line − experiment, second line − theoretical calculation; ρ is the electron density; $\nabla^2\rho$ is the Laplacian; R_{ij} is interatomic distance, d_1 and d_2 are the distances from the critical point to atoms 1 and 2, λ_1, λ_2, λ_3 are the principal curvatures, ϵ is bond ellipticity, n_{topo} is topological bond order. [b] Symmetry operator: $(1-x, -y, 1-z)$.

S···N in 1,5-triazocine;[49] S···S in S_8^{2+};[50,51] Se···Se in Se_8^{2+} [50] and N···N in tetranitrogen dianions.[52] The C···C interactions in [2.2]paracyclophane[53] and Si···N in 1-methylsilatrane[54] have been analyzed based on both experimental and theoretical data. The N···N critical point properties reported here are slightly smaller than in ref 52, which correlates with the longer N−N distance.

Eight moderately strong hydrogen bonds (of the type C−H···O) have been found in the β-HMX crystal (Figure 2); the properties of the corresponding bond critical points are listed in Table 3. The interatomic distances for these hydrogen bonds vary between 2.32 and 2.94 Å, and the dissociation energies vary between 1.8 and 8.9 kJ/mol as determined from the potential energy density at the critical point.[55] Despite the existence of two short O···H intramolecular contacts in the β-HMX molecule[9] (2.19 and 2.37 Å), no critical points associated with these possible interactions were located. Weaker C···O and O···O[56] bonding interactions have also been found in the β-HMX crystal. For every interaction listed in Tables 2 and 3, a bond path and the associated virial path have been found, which demonstrate the bonding character of these interactions[43]. All the explosive materials studied with the QTAIM analysis[31−35,56−59] so far are particularly rich in closed-shell intra- and interatomic interactions.

Table 4 lists the atomic volumes, charges, and total electronic energies integrated over the atomic basins delimited by the zero-flux surfaces for the experimental data and the solid-state calculation. The integrated Lagrangian for every atom was reasonably small, demonstrating the accuracy of the integrations. All of the atomic charges sum to very small values thus confirming that the molecule is practically electroneutral as required. The sums of the atomic volumes reproduce the unit cell volume per molecule with an error of 0.1%. We have also calculated the atomic charges and volumes for the β-HMX procrystal again using zero-flux surface partitioning.[60] These procrystal "atomic charges" are significantly different from zero and have the same signs as charges in a real crystal. The "deformation charges", $\delta q = q - q^{pro}$, reflect the interatomic electron transfer which accompanies the molecule and crystal formation.[57] These charges are generally smaller than the total atomic charges. In the same way, the differences in atomic volumes, $\delta\Omega$, reflect how the atomic volumes change upon formation of the molecule or crystal from neutral atoms. The oxygen atoms, and nitrogens in the ring (N(2) and N(3)) become much more negative, and their atomic volumes are increased,

(49) Jalsovszky, I.; Farkas, Ö.; Kuksman, À. *J. Mol. Struct. THEOCHEM* **1997**, *418*, 155−163.
(50) Cameron, T. S.; Deeth, R. J.; Dionne, I.; Du, H.; Jenkins, H. D. B.; Krossing, I.; Passmore, J.; Roobottom, H. K. *Inorg. Chem.* **2000**, *39*, 5614−5631.
(51) Tang, T. -H.; Bader, R. F. W.; MacDougall, P. J. *Inorg. Chem.* **1985**, *24*, 2047−2053.
(52) Geier, J.; Grützmacher, H.; Exner, K.; Prinzbach, H. *Angew. Chem.* **2005**, *44*, 2433−2437.
(53) Lyssenko, K. A.; Antipin Yu, M.; Antonov Yu, D. *Chemphyschem* **2003**, *4*, 817−823.
(54) Lyssenko, K. A.; Korlyukov, A. A.; Antipin Yu, M.; Knyazev, S. P.; Kirin, V. N.; Alexeev, N. V.; Chernyshev, E. A. *Mendeleev Comm.* **2000**, *2*, 83−124.
(55) Espinosa, E.; Molins, E. *J. Chem. Phys.* **2000**, *11*, 5686−5694.
(56) Zhurova, E. A.; Tsirelson, V. G.; Stash, A. I.; Pinkerton, A. A. *J. Am. Chem. Soc.* **2002**, *124*, 4574−4575.
(57) Zhurova, E. A.; Tsirelson, V. G.; Stash, A. I.; Yakovlev, M. V.; Pinkerton, A. A. *J. Phys. Chem.* **2004**, *B108*, 20173−20179.
(58) Pinkerton, A. A.; Zhurova, E. A.; Chen, Yu.-Sh. In *Energetic Materials. Theoretical and Computational Chemistry Series*; Politzer, P., Murray, J. S., Eds.; Elsevier: New York 2003; Vol. 12, pp 215−245.
(59) Klapötke, T. M.; Mayer, P.; Schulz, A.; Weigand, J. J. *J. Am. Chem. Soc.* **2005**, *127*, 2032−2033.
(60) Maslen, E. N.; Spackman, M. A. *Aust. J. Phys.* **1985**, *38*, 273−287.

Table 3. Bond Critical Points in the β-HMX Crystal: Closed-shell Interactions[a]

bond	ρ, eÅ^{-3}	$\nabla^2\rho$, eÅ^{-5}	R_{ij}, Å	d_1, Å	d_2, Å	λ_1, eÅ^{-5}	λ_2, eÅ^{-5}	λ_3, eÅ^{-5}	g, a.u.	v, a.u.	h_e, a.u.	D_e, kJ/mol
N(2)−N(2)[b]	0.116	1.71	2.744	1.372	1.372	−0.307	−0.055	2.072	0.0151	−0.0125	0.0026	16.41
	0.118	1.73	2.744	1.372	1.372	−0.311	−0.099	2.144	0.0154	−0.0128	0.0026	16.76
O(4)−H(2A)[c]	0.078	0.99	2.317	1.379	0.943	−0.338	−0.322	1.647	0.0085	−0.0068	0.0017	8.93
	0.074	1.06	2.317	1.381	0.937	−0.292	−0.269	1.622	0.0089	−0.0068	0.0021	8.93
O(3)−H(1A)[d]	0.050	0.99	2.431	1.429	1.031	−0.185	−0.149	1.323	0.0077	−0.0051	0.0026	6.70
	0.057	0.98	2.431	1.416	1.025	−0.212	−0.165	1.354	0.0078	−0.0054	0.0024	7.09
O(3)−H(2B)[e]	0.053	0.89	2.391	1.422	0.971	−0.200	−0.183	1.272	0.0070	−0.0049	0.0022	6.43
	0.061	0.88	2.391	1.411	0.981	−0.231	−0.213	1.324	0.0072	−0.0053	0.0019	6.96
O(2)−H(2A)[f]	0.047	0.82	2.601	1.453	1.254	−0.135	−0.040	0.997	0.0064	−0.0043	0.0021	5.64
	0.053	0.83	2.601	1.442	1.235	−0.151	−0.075	1.053	0.0066	−0.0047	0.0020	6.17
O(1)−H(1B)[f]	0.037	0.67	2.570	1.531	1.049	−0.127	−0.085	0.886	0.0052	−0.0033	0.0018	4.33
	0.040	0.66	2.570	1.500	1.072	−0.143	−0.103	0.907	0.0051	−0.0034	0.0017	4.46
O(4)−H(1A)[c]	0.043	0.65	2.531	1.497	1.036	−0.159	−0.127	0.932	0.0052	−0.0035	0.0016	4.59
	0.046	0.64	2.531	1.477	1.055	−0.163	−0.142	0.943	0.0051	−0.0036	0.0015	4.73
O(1)−H(2B)[e]	0.039	0.80	2.503	1.469	1.041	−0.120	−0.108	1.030	0.0061	−0.0038	0.0022	4.99
	0.047	0.76	2.503	1.455	1.049	−0.158	−0.139	1.060	0.0060	−0.0041	0.0019	5.38
O(1)−H(2A)[c]	0.018	0.33	2.936	1.653	1.385	−0.042	−0.008	0.377	0.0024	−0.0014	0.0010	1.84
	0.019	0.34	2.936	1.650	1.314	−0.045	−0.021	0.402	0.0025	−0.0015	0.0010	1.97
O(2)−C(1)[f]	0.056	1.00	2.935	1.457	1.486	−0.117	−0.062	1.176	0.0079	−0.0054	0.0025	7.09
	0.060	0.96	2.935	1.437	1.501	−0.117	−0.070	1.147	0.0077	−0.0055	0.0022	7.22
O(1)−O(4)[g]	0.045	0.74	3.017	1.495	1.527	−0.127	−0.090	0.958	0.0058	−0.0039	0.0019	5.12
	0.042	0.74	3.017	1.502	1.520	−0.114	−0.078	0.931	0.0057	−0.0038	0.0020	4.99
O(1)−O(4)[h]	0.042	0.71	3.008	1.534	1.485	−0.132	−0.068	0.915	0.0055	−0.0037	0.0019	4.86
	0.042	0.72	3.008	1.563	1.481	−0.139	−0.035	0.897	0.0056	−0.0037	0.0019	4.86
O(2)−O(3)[i]	0.036	0.65	3.038	1.522	1.518	−0.101	−0.094	0.842	0.0050	−0.0032	0.0018	4.20
	0.036	0.65	3.038	1.522	1.517	−0.104	−0.089	0.839	0.0049	−0.0032	0.0018	4.20
O(3)−O(4)[j]	0.022	0.40	3.249	1.622	1.628	−0.065	−0.056	0.523	0.0030	−0.0018	0.0012	2.36
	0.021	0.38	3.249	1.622	1.629	−0.060	−0.040	0.476	0.0028	−0.0017	0.0011	2.23
O(2)−O(3)[k]	0.013	0.23	3.424	1.724	1.700	−0.032	−0.026	0.286	0.0017	−0.0010	0.0007	1.31
	0.014	0.24	3.424	1.715	1.708	−0.035	−0.026	0.302	0.0018	−0.0010	0.0007	1.31

[a] First line − experiment, second line − theoretical calculation; ρ is the electron density; $\nabla^2\rho$ is the Laplacian; R_{ij} is the interatomic distance, d_1 and d_2 are the distances from the critical point to atoms 1 and 2, λ_1, λ_2, λ_3 are the principal curvatures, g, v and h_e are the kinetic, potential, and total electronic energies at the critical point, respectively. D_e is an approximate dissociation energy[55] calculated as $D_e = -v/2$. All bond paths and virial paths have been verified. [b] Symmetry operator: $(1-x, -y, 1-z)$. [c] Symmetry operator: $(1+x, y, z)$. [d] Symmetry operator: $(1-x, -y, -z)$. [e] Symmetry operator: $(1/2+x, 1/2-y, -1/2+z)$. [f] Symmetry operator: $(1/2+x, 1/2-y, 1/2+z)$. [g] Symmetry operator: $(3/2-x, 1/2+y, 1/2-z)$. [h] Symmetry operator: $(2-x, -y, 1-z)$. [i] Symmetry operator: $(-1/2+x, 1/2-y, 1/2+z)$. [j] Symmetry operator: $(2-x, -y, -z)$. [k] Symmetry operator: $(x, y, 1+z)$.

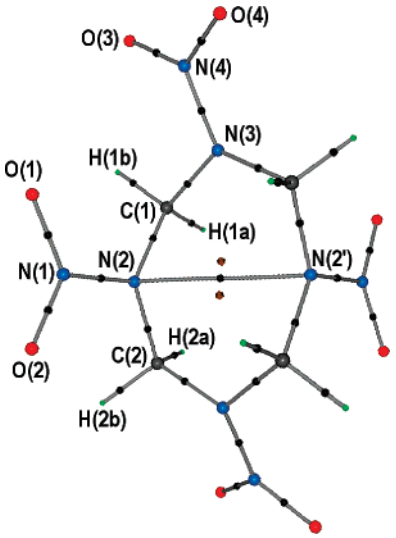

Figure 4. β-HMX molecular graph. Atoms are shown as colored balls with sizes proportional to their covalent radii, (3,−1) critical points are shown as black balls, and (3,+1) points are shown as brown cubes, bond paths are gray.

as anticipated. Carbon atoms, and nitrogens of the NO_2 groups (N(1) and N(4)) become more positive, and their atomic volumes become smaller; whereas for the hydrogen atoms the deformation charges are close to zero, and their volumes only slightly decrease during crystal formation. The sums of the total electronic energies integrated over the atomic basins[57,61] agree well with the total energies calculated with wave-functions using CRYSTAL98 (within 0.05%). The β-HMX molecular electronic energy per mole H_e/M is 4.04 a.u.; this situates HMX in the middle of the range previously reported for other energetic compounds.[35] Its shock sensitivity (h_{50} = 26, 29, 32 cm) is also "medium". As a bigger sample of compounds studied with QTAIM becomes available, we anticipate that it will become possible to relate atomic group properties and dissociation energies with impact sensitivities of explosive materials.

The electrostatic potential (ESP) was calculated from the experimental electron density[63] for a single β-HMX molecule taken from crystal. The ESP distribution mapped onto a molecular surface, defined as the electron density isosurface of 0.001 a.u., is shown in Figure 5. Other ESP maps have been deposited. An excellent agreement between experimental and theoretical electrostatic potentials is observed. This ESP distribution is in good qualitative agreement with the earlier theoretically calculated electrostatic potential pattern for a single β-HMX molecule[64] and is typical for a moderately shock sensitive explosive. The expected negative regions around the nitro-groups and a positive core are observed. Oxygen atoms of closely located NO_2 groups form continuous negative regions on the molecular surface (Figure 5), which is an indication of a cooperative effect. These regions represent the sites of possible electrophilic attack.

(61) Tsirelson, V. G.; Stash, A. I. *Acta Cryst.* **2004**, *A60*, 418−426.
(62) Flensburg, C.; Madsen, D. *Acta Cryst.* **2000**, *A56*, 24−28.
(63) Su, Z.; Coppens, P. *Acta Cryst.* **1992**, *A48*, 188−197.
(64) Rice, B. M.; Hare, J. J. *J. Phys. Chem.* **2002**, *A106*, 1770−1783.
(65) The *gOpenMol* program (www.csc.fi/gopenmol).

Table 4. Atomic Charges (q), Volumes (Ω) and Total Electronic Energies (H_e) Integrated over Atomic Basins[a]

atom	q, e$^-$	$q^{procrystal}$, e$^-$	δq, e$^-$	Ω, Å^3	$\Omega^{procrystal}$, Å^3	$\delta\Omega$, Å^3	$-H_e$, a.u.
O(1)	−0.385	−0.188	−0.197	14.82	13.35	1.47	75.163
	−0.387	−0.188	−0.199	14.66	13.35	1.31	75.139
O(2)	−0.390	−0.195	−0.195	15.14	13.64	1.50	75.169
	−0.391	−0.195	−0.196	14.95	13.64	1.31	75.140
O(3)	−0.376	−0.202	−0.174	15.58	14.13	1.45	75.143
	−0.389	−0.202	−0.187	15.47	14.13	1.34	75.142
O(4)	−0.407	−0.192	−0.215	14.88	13.45	1.43	75.207
	−0.404	−0.192	−0.212	14.75	13.45	1.30	75.168
N(1)	0.529	0.295	0.234	6.71	7.42	−0.71	54.418
	0.605	0.295	0.310	6.62	7.42	−0.80	54.305
N(2)	−0.553	−0.350	−0.203	8.69	8.00	0.69	55.269
	−0.516	−0.350	−0.166	8.61	8.00	0.61	55.230
N(3)	−0.548	−0.324	−0.224	9.77	9.01	0.76	55.260
	−0.504	−0.324	−0.180	9.66	9.01	0.65	55.224
N(4)	0.511	0.290	0.221	6.65	7.32	−0.67	54.463
	0.601	0.290	0.312	6.50	7.32	−0.82	54.311
C(1)	0.456	0.135	0.321	6.80	8.37	−1.57	38.125
	0.403	0.135	0.268	6.85	8.37	−1.52	38.232
C(2)	0.432	0.134	0.298	6.94	8.51	−1.57	38.151
	0.413	0.134	0.279	6.87	8.51	−1.64	38.213
H(1a)	0.151	0.149	0.002	4.85	5.50	−0.65	0.558
	0.141	0.149	−0.008	5.04	5.50	−0.46	0.554
H(1b)	0.219	0.154	0.065	4.85	5.70	−0.85	0.498
	0.148	0.154	−0.006	5.31	5.70	−0.39	0.547
H(2a)	0.166	0.152	0.014	4.71	5.27	−0.40	0.541
	0.128	0.152	−0.024	4.92	5.27	−0.35	0.563
H(2b)	0.198	0.154	0.044	4.80	5.45	−0.37	0.513
	0.152	0.154	−0.002	4.99	5.45	−0.46	0.546
whole	0.007	0.021	−0.014	250.38	250.24	0.14	1196.956
molecule	0.000	0.021	−0.021	250.40	250.24	0.16	1196.628

[a] First line − experiment, second line − solid state theoretical calculation; $\Omega_{unit\ cell}/2 = 250.69$ Å^3; $H_e^{Crystal98}/2 = -1196.331$ a.u.; $L_{err}^{molecule} = 0.0004$ a.u. (experiment), 0.0005 a.u. (theory), 0.0009 a.u. (procrystal), $L_{err} = (\Sigma L_\Omega^2/N_{atoms})^{1/2}$, L_Ω is the atomic integrated Lagrangian.[62]

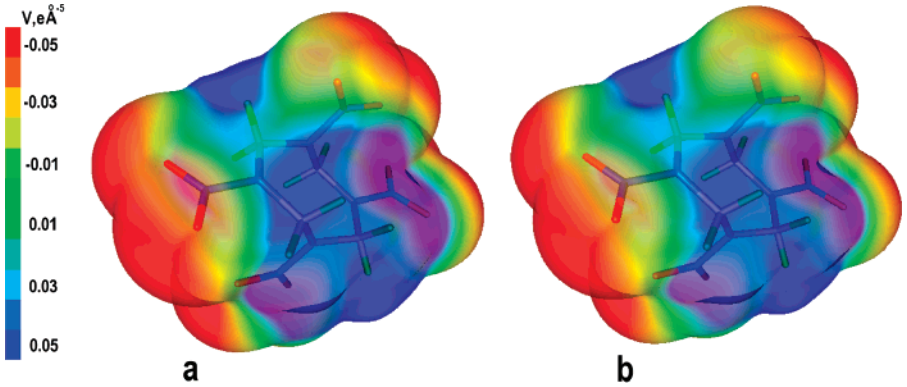

Figure 5. Electrostatic potential mapped onto the molecular surface ($\rho = 0.001$ a.u. $= 0.00675$ eÅ^{-3}): (a) calculated from the experimental electron density, (b) calculated from solid state theory. Color scheme ranges from red (−0.05 eÅ^{-1}) via green (0) to blue (0.05 eÅ^{-1}) (−16.1−16.1 kcal/(e•mol). The graphical program *gOpenMol*[65] was used to plot the data.

Conclusion

This paper reports accurately determined topological properties of the electron density and the electrostatic potential of the energetic β-HMX crystal. Expected conjugation of the electron density in the $-N-NO_2$ fragment was observed. Oxygen atom lone pair electron concentrations were found located almost perpendicular to N−O bond vectors. In addition to covalent bonds in the β-HMX molecule, an N(2)···N(2) bonding closed-shell interaction across the 8-membered ring has been discovered. The dissociation energy of this interaction is ∼17 kJ/mol. Hydrogen bonding was found to be moderately strong in the β-HMX crystal, with dissociation energies varying between 1.8 and 8.9 kJ/mol. O···O and O···C intermolecular interactions were also found and characterized. The β-HMX molecular electronic energy per mole H_e/M is 4.04 a.u., thus fitting into the middle of the range for known energetic compounds. Asymmetry in the electrostatic potential due to the proximity of two nitro-groups is also demonstrated.

Acknowledgment. This work was supported by the Office of Naval Research through the contract number N00014-07-1-0314.

Supporting Information Available: Complete ref 46, CIF-file, experimental reflection statistics, residual and deformation electron density maps, Laplacian and electrostatic potential maps. This material is available free of charge via the Internet at http://pubs.acs.org.

JA073801B